NASA TECHNICAL NOTE

NASA TN D-6916

COOLANT PRESSURE AND AIRFLOW DISTRIBUTION IN A STRUT-SUPPORTED TRANSPIRATION-COOLED VANE FOR A GAS TURBINE ENGINE

by Albert Kaufman, David J. Poferl, and Hadley T. Richards

Lewis Research Center
Cleveland, Ohio 44135

NATIONAL AERONAUTICS AND SPACE ADMINISTRATION • WASHINGTON, D. C. • AUGUST 1972

1. Report No.	2. Government Accession No.	3. Recipient's Catalog No.
NASA TN D-6916		

4. Title and Subtitle	5. Report Date
COOLANT PRESSURE AND AIRFLOW DISTRIBUTION IN A STRUT-SUPPORTED TRANSPIRATION-COOLED VANE FOR A GAS TURBINE ENGINE	August 1972
	6. Performing Organization Code
7. Author(s)	8. Performing Organization Report No.
Albert Kaufman, David J. Poferl, and Hadley T. Richards	E-6800
	10. Work Unit No.
9. Performing Organization Name and Address	764-74
Lewis Research Center National Aeronautics and Space Administration Cleveland, Ohio 44135	11. Contract or Grant No.
	13. Type of Report and Period Covered
12. Sponsoring Agency Name and Address	Technical Note
National Aeronautics and Space Administration Washington, D.C. 20546	14. Sponsoring Agency Code

15. Supplementary Notes

16. Abstract

An analysis to predict pressure and flow distribution in a strut-supported wire-cloth vane was developed. Results were compared with experimental data obtained from room-temperature airflow tests conducted over a range of vane inlet airflow rates from 10.7 to 40.4 g/sec (0.0235 to 0.0890 lb/sec). The analytical method yielded reasonably accurate predictions of vane coolant flow rate and pressure distribution.

17. Key Words (Suggested by Author(s))	18. Distribution Statement
Turbine cooling Transpiration cooling Fluid flow	Unclassified - unlimited

19. Security Classif. (of this report)	20. Security Classif. (of this page)	21. No. of Pages	22. Price*
Unclassified	Unclassified	25	$3.00

* For sale by the National Technical Information Service, Springfield, Virginia 22151

COOLANT PRESSURE AND AIRFLOW DISTRIBUTION IN A STRUT-SUPPORTED TRANSPIRATION-COOLED VANE FOR A GAS TURBINE ENGINE

by Albert Kaufman, David J. Poferl, and Hadley T. Richards

Lewis Research Center

SUMMARY

Analytical predictions and experimental studies were made of the coolant flow and pressure distributions in a transpiration-cooled vane. The vane consisted of a wire-form porous airfoil shell joined to a cast strut. The coolant was distributed to the porous shell through spanwise coolant passages in the strut surface; these passages, in turn, were fed through metering orifices from a common plenum at the tip shroud.

The prediction method was based on (1) a flow balance of the coolant in each passage, (2) an empirical correlation for flow characteristics of the porous material, (3) compressible flow relations that accounted for contraction and expansion effects for flow through the orifices, (4) empirically determined orifice discharge coefficients, and (5) a one-dimensional momentum analysis for a passage with variable areas, temperatures, pressures, and flow ejection. Predictions were compared with results of room-temperature flow tests conducted over a range of vane inlet flow rates from 10.7 to 40.4 g/sec (0.0235 to 0.0890 lb/sec). There was generally good agreement between experimental and predicted results.

INTRODUCTION

An analysis to predict flow and pressure distributions in a strut-supported wire-cloth vane was developed, and experimental flow and pressure data were compared with predicted results. Coolant was distributed to the porous shell from a common plenum at the tip shroud through thick-plate metering orifices into spanwise-oriented passages along the strut surface. The vane was designed for operation in the NASA cascade and engine facilities described in reference 1 at a turbine inlet temperature of 1644 K (2500° F) with 922 K (1200° F) air at 31 N/cm^2 (45 psia).

Prediction of the heat transfer performance of a transpiration-cooled vane requires detailed knowledge of the coolant flow and pressure distributions throughout the vane. This study is part of a series of studies undertaken by the Lewis Research Center to investigate flow distributions in various types of vanes, blades, and flow models. In a previous study (ref. 2), the coolant flow through a predominantly convection-cooled vane with trailing-edge pin fins and leading-edge impingement cooling was investigated. Reference 3 describes flow model tests in which the discharge coefficients for thick-plate orifices were determined.

The purpose of this study was to develop a procedure for predicting the flow distribution and pressure losses in a transpiration-cooled vane with a strut-supported, wire-form porous shell. The prediction method was based on a flow balance of each passage and used empirical discharge coefficient relations for the metering orifices at the entrances of the coolant passages (ref. 3), compressible flow solutions for contraction and expansion effects due to flow through the orifices (ref. 4), a one-dimensional momentum analysis for a passage with variable mass flows (ref. 2), and the flow equation for porous media (ref. 5) together with the nominal flow characteristics of the porous airfoil shell (ref. 6).

Accuracy of the analytical method was verified in a bench-type flow facility by comparison with results of room-temperature flow tests on an instrumented vane. Experimental data from a typical flow test with a vane inlet supply flow rate of 33.2 grams per second (0.0731 lb/sec) were compared with pressure and flow predictions. Similar results were obtained from other runs but are not reported herein.

SYMBOLS

A	area
A to J	orifice or passage designation
C_d	orifice discharge coefficient
D_h	hydraulic diameter
f	D'Arcy-Weisbach friction factor
G	mass flow rate per unit area
g	universal gravitational constant
M	Mach number
P	static pressure
P'	total pressure

R	gas constant
Re	Reynolds number
T	static temperature
V	velocity
$\dot{w}$	mass flow rate
x	passage distance from orifice
α	viscous resistance coefficient
β	inertial resistance coefficient
β_{in}	ratio of hydraulic diameters of orifice and plenum
β_{out}	ratio of flow areas of orifice and passage
γ	ratio of specific heats
μ	viscosity
ρ	density
τ	porous material thickness

Subscripts:

A	region A of fig. 5
atm	atmospheric
o	orifice
p	passage
s	porous shell
1	plenum
2	orifice exit
3	reattachment point in passage

EXPERIMENTAL APPARATUS AND PROCEDURE

Vane Description

The transpiration-cooled vane used in this study was designed by the Detroit Diesel Allison Division of General Motors Corporation (ref. 7). This vane is shown in figure 1 both before and after the porous shell was welded to the strut. The vane had a span of

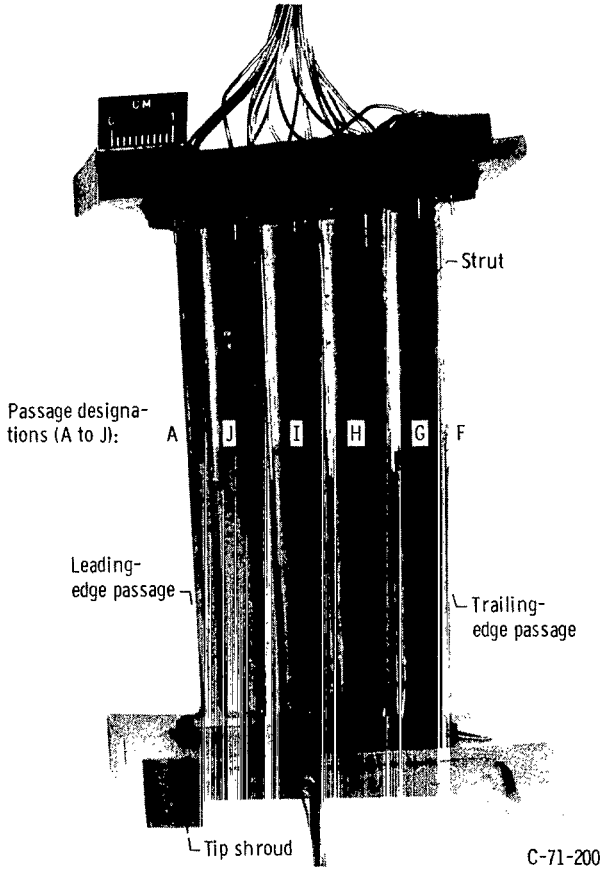

(a) Before porous shell was welded to strut - pressure side.

Figure 1. - Transpiration-cooled vane.

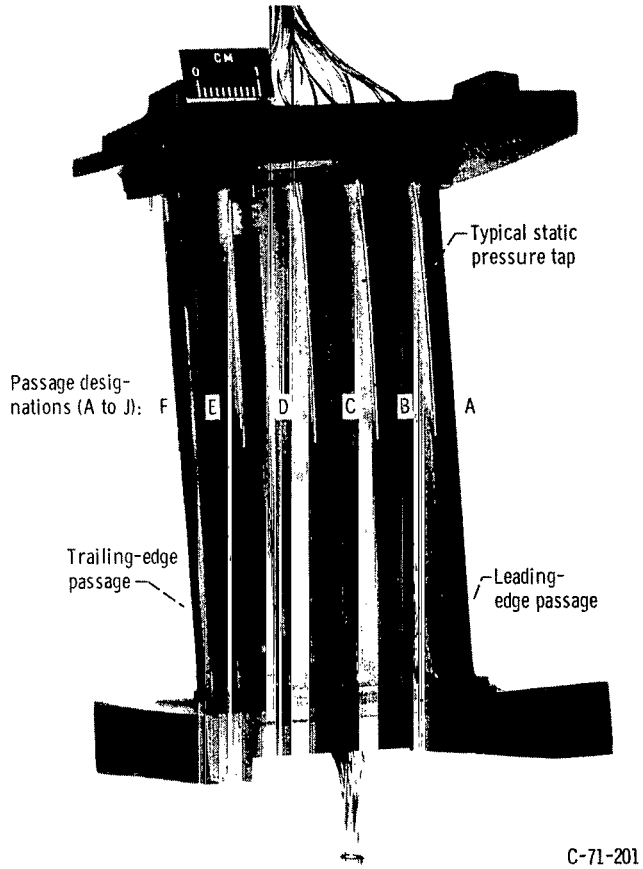

(b) Before porous shell was welded to strut - suction side.

Figure 1. - Continued.

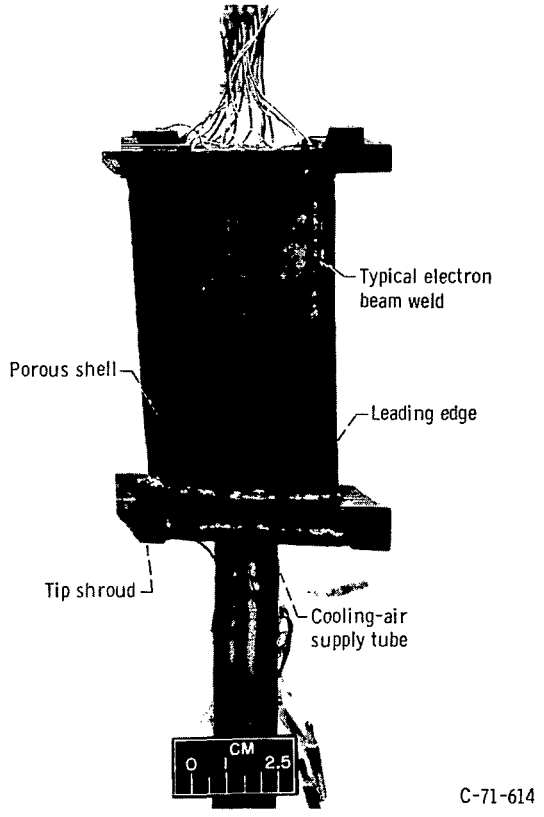

(c) After porous shell was welded to strut.

Figure 1. - Concluded.

about 10 centimeters (4 in.) and a chord of about 6.4 centimeters (2.5 in.). The porous airfoil shell was fabricated from Poroloy, a wire-wound porous material manufactured by the Bendix Corporation. The Poroloy was wound from Driver-Harris 242 wire to a thickness of 0.061 centimeter (0.024 in.) and to a nominal standard flow rate of 3.52 kg/sec-m^2 (5.0×10^{-3} lb/sec-$in.^2$) based on standard conditions of 17.0 N/cm^2 (24.7-psia) inlet pressure, 10.1-N/cm^2 (14.7-psia) discharge pressure, and 294 K (70° F).

The Poroloy was joined to the strut at lands between cooling passages and around the airfoil hub and tip ends by electron beam welding. At the trailing edge, the ends of the Poroloy shell were spot-welded together.

Cooling air was supplied to the vane through a tube attached to the tip shroud. The air impinged on a baffle plate and entered a plenum chamber in the shroud (as shown in fig. 2) and was distributed to 10 spanwise coolant passages (designated A to J) through electrical-discharge-machined metering orifices. The baffle plate was supposed to have been positioned to cover all the orifices under the inlet tube. However, due to a fabrication error, it was installed such that orifices H and I were exposed, as shown in figure 2. Views of the suction- and pressure-side coolant passages are shown in fig-

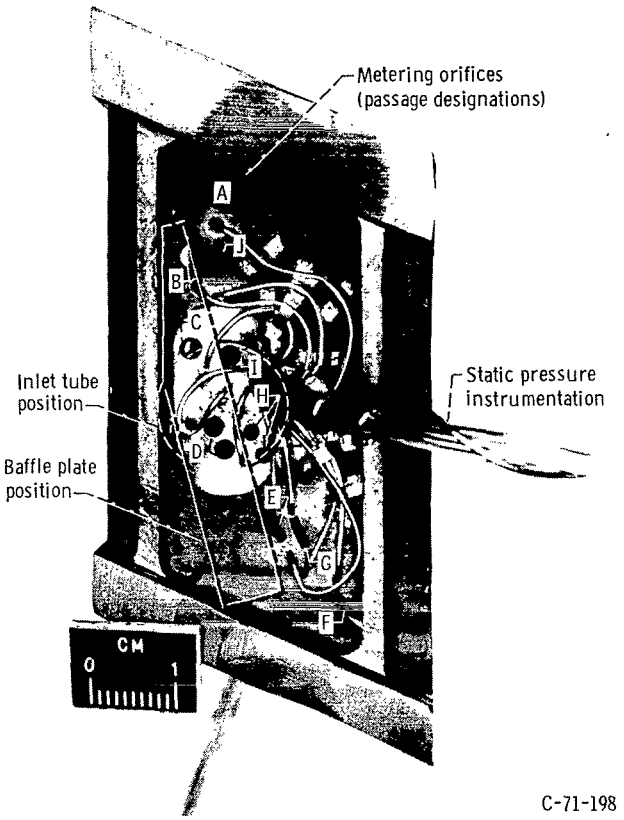

Figure 2. - Vane metering orifices in tip shroud.

ures 1(a) and (b). The two passages on the suction side nearest the trailing edge (designated passages D and E) are interconnected. The shapes of the metering orifices are shown in figure 2, which is a view into the tip shroud plenum before the supply tube was attached. (The orifices are lettered to correspond with vane cooling passage designation.) The trailing-edge opening (F) was essentially triangular in shape and had the same shape and flow area as the passage itself. Rectangular orifices (E and G) were machined for the two small passages immediately adjacent to the trailing edge in order to obtain sufficient metering flow area to these passages. Passages D and H were also small and required two circular orifices. The five passages (A, B, C, J, and I) nearest the leading edge were large enough that coolant could be supplied through single circular orifices.

As air flowed through a passage, it was progressively ejected through the porous skin. The coolant passages were approximately 9 centimeters (3.6 in.) long and were formed either by cast depressions in the strut or, in the case of the leading- and trailing-edge passages, by providing gaps between the strut and shell. The orifice and passage areas and hydraulic diameters, as well as the passage flow widths are shown in table I. Orifice lengths varied from 0.87 to 1.07 centimeters (0.34 to 0.42 in.).

TABLE I. - VANE PASSAGE AND ORIFICE DIMENSIONS

Cooling passage	Orifice dimensions				Passage dimensions					
	Area, A_o		Hydraulic diameter, $D_{h,o}$		Area, A_p		Hydraulic diameter, $D_{h,p}$		Flow width	
	cm^2	$in.^2$	cm	in.	cm^2	$in.^2$	cm	in.	cm	in.
A	0.2187	0.0339	0.528	0.208	0.3858	0.0598	0.643	0.253	1.628	0.641
B	.0806	.0125	.320	.126	.3097	.0480	.516	.203	.940	.370
C	.0594	.0092	.274	.108	.2806	.0435	.333	.131	.879	.346
D-E	.1561	.0242	.244	.096	.4348	.0674	.488	.192	2.395	.943
F	.0903	.0140	.244	.096	.0903	.0140	.203	.080	1.173	.463
G	.0529	.0082	.196	.077	.0800	.0124	.193	.076	.663	.261
H	.0568	.0088	.191	.075	.2419	.0375	.384	.151	.876	.345
I	.0561	.0087	.267	.105	.2542	.0394	.455	.179	.879	.346
J	.0561	.0087	.267	.105	.3065	.0475	.503	.198	.909	.358

Flow Apparatus

A schematic diagram of the bench-type flow facility and the associated instrumentation used for this investigation is shown in figure 3. Room-temperature air at 86.2 N/cm^2 (125 psig) was supplied to the test vane through a dryer and filter, two pressure

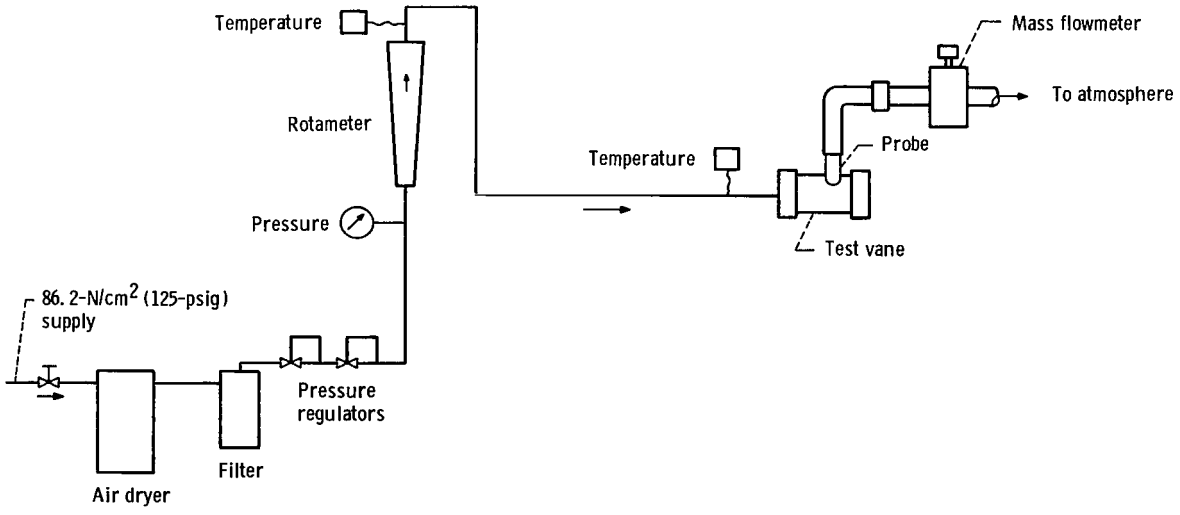

Figure 3. - Bench-type vane flow facility.

regulators in series, and a rotameter.

Local airflow through the porous shell was collected by a probe made from acrylic plastic tubing and was measured in a calibrated flowmeter. The flowmeter consisted of a hot-wire anemometer in a venturi to permit linearized mass flow readings. A different probe was used for each passage. Each probe was formed to the contour of the airfoil at the chordwise measurement location. In order to minimize leakage around the rim of the probe, the backpressure within it was maintained at approximately atmospheric pressure.

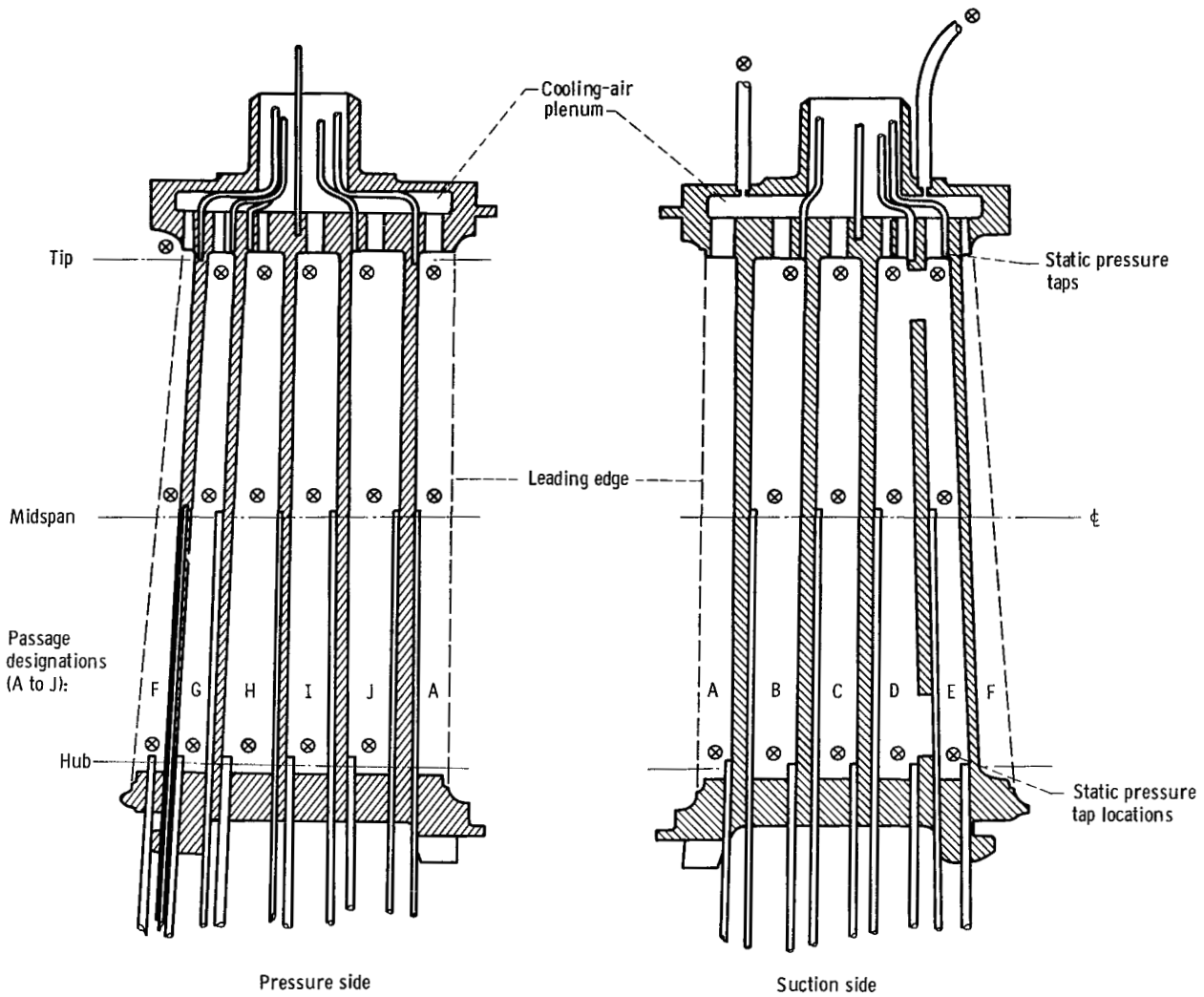

Figure 4. - Vane static pressure measurement instrumentation.

Instrumentation

A total of 32 static pressure taps were attached to the test vane. The locations of these taps are shown in figure 4. Pressure taps were located on the strut at the hub, midspan, and tip of each of the 10 coolant passages (A to J). In addition, two pressure taps were located in the tip shroud plenum chamber. The accuracy of the pressure measurements was assumed to be ± 0.034 N/cm^2 (± 0.05 psi).

The inlet airflow was measured by a rotameter connected to the inlet supply tube. The exit airflow rate from the porous shell at any location was measured by a hot-wire anemometer flowmeter (model 1352-3, Thermo-Systems, Inc.). Accuracies were assumed to be 0.5 percent of full scale for the rotameter and 0.2 percent of full scale for the hot-wire anemometer.

The inlet air temperature was measured by inserting a thermocouple probe in the airstream through the supply tube. The thermocouple was read on a null balance potentiometer to 2.8 K (5° F).

Test Procedure

Flow tests were conducted on the test vane at inlet flow rates from 10.7 to 40.4 g/sec (0.0235 to 0.0890 lb/sec). The accuracy of the prediction method was verified by comparison with experimental data obtained at an inlet flow rate of 33.2 g/sec (0.0731 lb/sec), which was about the maximum flow rate of interest for the transpiration-cooled vane. Similar comparisons were also made for other inlet flow rates but are not reported herein.

At each of these test conditions, flow rate measurements using plastic tube probes were made at seven span locations on the porous shell over each cooling passage. For the leading- and trailing-edge passages (A and F, respectively, in fig. 4), probe measurements were taken on both the suction- and pressure-surface sides. The span locations at which the measurements were made were as close to the ends of the passages as practicable and at approximately 1.27-centimeter (0.50-in.) increments between. The flow characteristics of the Poroloy vane shell were determined by the procedure described in reference 6 for the hub midspan and tip of each passage. These locations were selected because they coincided with the locations of the pressure taps in the passages.

Analytical Procedure

The airflow rate distribution in the vane was calculated by a method which involved the balancing of the airflow into and out of each passage so that there was essentially zero flow at the end of the passage. The input data required for this computation were (1) the plenum pressure; (2) the flow and pressure drop characteristics of the porous shell, α and β; (3) the dimensions of the orifices and passages which are given in table I; and (4) the orifice discharge coefficients. For the purpose of this analysis, passages D and E in figure 4, which were interconnected, were considered to be one passage.

A flow model of a typical coolant passage is shown in figure 5. Region A, which was estimated to extend over a distance of seven passage hydraulic diameters from the orifice exit (based on results presented in ref. 8), is the portion of the passage associated with the expansion loss due to the air flowing into an abrupt enlargement. The static pressure in this region was assumed to vary linearly from the static pressure

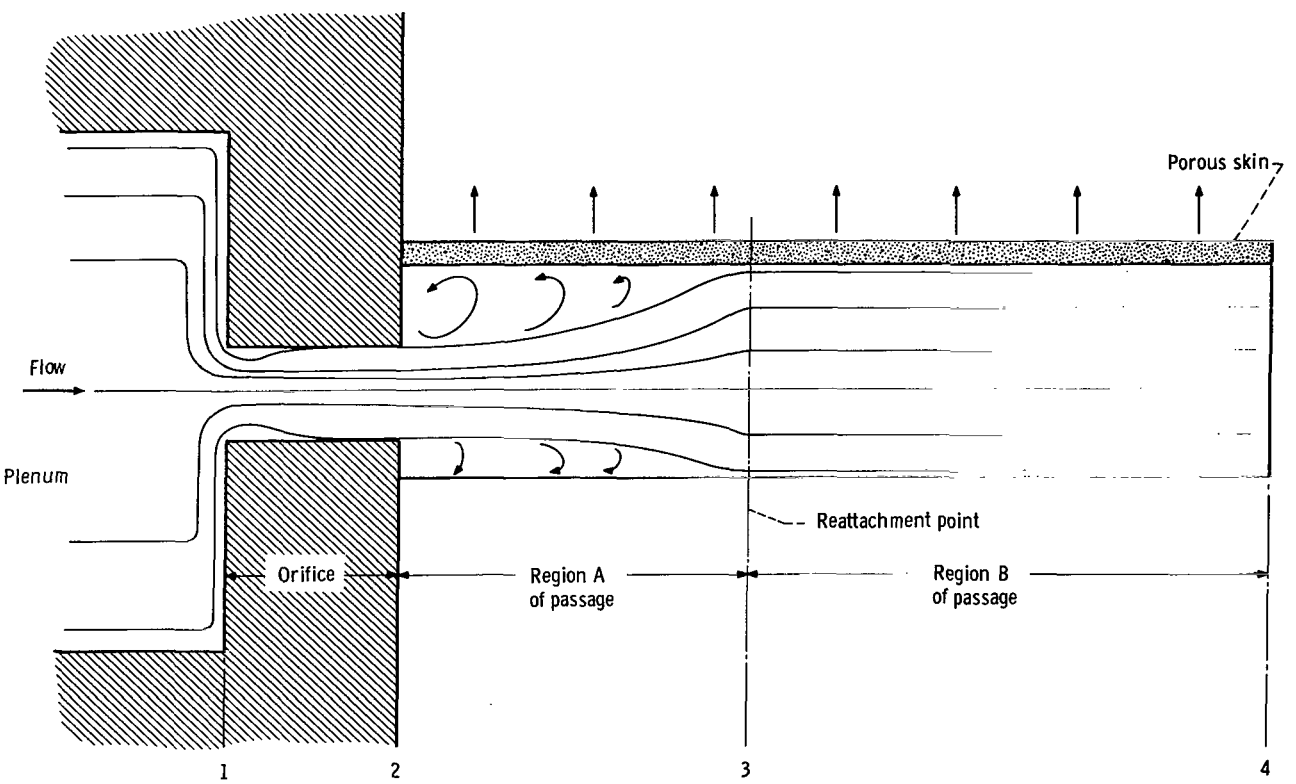

Figure 5. - Flow model of coolant passage.

at the orifice exit jet (station 2) to the static pressure at the reattachment point (station 3), where the flow completely fills the passage. This assumption of linearity approximates the recovery data presented in reference 8. In region B, the remainder of the passage, completely recovered flow was assumed to exist. This model applied to all passages except passage F. The model for passage F was modified to account for the fact that there was no abrupt expansion as the flow entered the passage since the orifice and passage areas were equal.

The following steps were followed to determine the flow and pressure distribution in each passage except passage F:

(1) An inlet flow rate through the metering orifice was assumed.

(2) An orifice discharge coefficient was obtained from experimental data shown in reference 3.

(3) The static pressure at the orifice exit was calculated from the orifice discharge coefficient.

(4) The loss in total pressure from the plenum to the orifice was calculated from compressible flow losses due to an abrupt contraction.

(5) The total pressure at the reattachment point (seven passage hydraulic diameters downstream of the orifice exit) was calculated from a compressible flow solution for an abrupt expansion.

(6) By using the orifice exit static pressure obtained from step 3, an initial estimate of the static pressure at station 3, the flow discharge equation for porous media, and the nominal flow characteristics of the wire-cloth shell as determined from reference 6, the flow distribution in region A was calculated based on the assumption of a linear change in static pressure from station 2 to station 3.

(7) An improved estimate of static pressure at the reattachment point was computed from the calculated value of passage coolant flow at station 3.

(8) Iteration was continued until convergence (based on static pressure at station 3) was obtained.

(9) The flow distribution and pressure losses in region B were calculated from the flow discharge equation for a porous media and from a one-dimensional compressible flow solution for a passage with flow ejection.

(10) Steps 1 to 9 were repeated until the flow rate at the end of the passage iterated to essentially zero.

Passage F was handled in the following manner: Steps 1 to 3 were used to obtain the static pressure at station 2. Step 9 was then used for the entire passage since there was no sudden expansion region in passage F. An iterative process using steps 1, 2, 3, and 9 was used until the coolant flow reached zero at the end of the passage (station 4).

Orifice Relations

The orifice discharge coefficients were defined as in reference 3:

$$C_d = \frac{\dot{w}_o}{\rho_2 V_2 A_o} \tag{1}$$

where

$$V_2 = \sqrt{\frac{2\gamma g RT}{\gamma - 1}\left[1 - \left(\frac{P_2}{P_1'}\right)^{(\gamma-1)/\gamma}\right]} \tag{2}$$

$$\rho_2 = \frac{P_2}{RT}\left(\frac{P_1'}{P_2}\right)^{(\gamma-1)/\gamma} \tag{3}$$

Pressure Relations

The total pressure loss across the orifice was determined from compressible flow relations for contraction and expansion effects caused by abrupt flow area changes (ref. 4).

The ratio of orifice to plenum total pressure was calculated from the following equation, which was obtained from a curve fit of the contraction loss curves shown in figure 12 of reference 4.

$$\frac{P_o'}{P_1'} = \left[\frac{P_2}{P_o'}\left(-0.587\,\beta_{in}^2 + 0.0399\,\beta_{in} + 0.572\right) + \left(0.587\,\beta_{in}^2 - 0.0399\,\beta_{in} + 0.428\right)\right] \tag{4}$$

where

$$\beta_{in} = \frac{D_{h,o}}{D_{h,1}} \tag{4a}$$

This relation applies where β_{in} is less than 0.3 and P_2/P_o' is greater than 0.75. The plenum hydraulic diameter was calculated to be 3.29 centimeters (1.29 in.).

The ratio of the total pressure at the reattachment point to the total pressure in the orifice can be written as

$$\frac{P'_3}{P'_o} = 1 - \left(1 - \frac{P_o}{P'_o}\right)\left(1 - \beta_{out}^2\right)^2 \tag{5}$$

where β_{out} is herein defined as $\sqrt{A_o/A_p}$ instead of the diameter ratio used in reference 4 because the former was found to give better results.

Equation (5) is applicable if P_2/P'_o is greater than 0.75.

The static pressure at the reattachment point was obtained from

$$P_3 = P'_3\left(1 + \frac{\gamma - 1}{2} M_3^2\right)^{-\gamma/(\gamma-1)} \tag{6}$$

where

$$M_3 = \frac{\dot{w}_3}{A_p P_3}\sqrt{\frac{RT}{\gamma g}} \tag{6a}$$

and

$$\dot{w}_3 = \dot{w}_o - \sum_A \Delta\dot{w}_s \tag{6b}$$

The summation of $\Delta\dot{w}_s$ is over region A of the passage and represents the total flow exiting through the wire cloth between station 2 and station 3. The calculation of $\Delta\dot{w}_s$ is described in the following section of this report.

For region B of figure 5, where the flow completely filled the passage, the static pressure at any point was predicted from the one-dimensional, compressible flow equation derived in reference 2 for the pressure drop in a passage with flow ejection. This equation is given here in finite difference form.

$$\Delta P = \left[\frac{-\left(\frac{RT}{gP}\right)\left(\frac{\dot{w}}{A_p}\right)\left(\frac{\Delta\dot{w}}{A_p\,\Delta x}\right) - \left(\frac{\dot{w}}{A_p}\right)^2\left(\frac{R}{gP}\right)\left(\frac{fT}{2D_{h,p}} + \frac{\Delta T}{\Delta x}\right)}{1 - \left(\frac{\dot{w}}{A_p}\right)^2\left(\frac{RT}{gP^2}\right)}\right]\Delta x \tag{7}$$

where for laminar flow

$$f = \frac{64}{(Re)_p} \tag{8}$$

and for turbulent flow

$$f = \frac{0.186}{(Re)_p^{0.2}} \tag{9}$$

Discharge Flow Relation

The equation for fluid flow through a porous media was derived by Green (ref. 5). This equation can be written in the form

$$\frac{P_p^2 - P_{atm}^2}{2\tau\mu RTG} g = \alpha + \beta\left(\frac{G}{\mu}\right) \tag{10}$$

where α and β are viscous and inertial resistance coefficients, respectively, defining the flow characteristics of the porous material. The resistance coefficients used for the calculations reported herein were determined from reference 6 by using the correlation equations for wire-form porous material. These equations gave an α-value of 7.717×10^{11} per square meter (4.979×10^{8}/in.^{2}) and a β-value of 1.050×10^{7} per meter (2.668×10^{5}/in.) for the specified standard flow rate of 3.52 kg/sec-m^2 (5.0×10^{-3} lb/sec-in.^{2}). The actual local resistance coefficients determined from vane flow tests ranged from 8.220×10^{11} to 12.82×10^{11} per square meter (5.303×10^{8} to 8.268×10^{8}/in.^{2}) for α and from 0.512×10^{7} to 3.448×10^{7} per meter (1.302×10^{-5} to 8.762×10^{5}/in.) for β. As demonstrated in reference 6 even apparently large variations in actual resistance coefficients from the nominal values usually make little difference in flow rate as the variations in α and β tend to go in opposite directions and to compensate for each other.

RESULTS AND DISCUSSION

Total Inlet and Discharge Airflow

Measured airflow rates through the vane inlet supply tube are compared with the measured total airflow discharge flow rate through the porous shell in figure 6. The

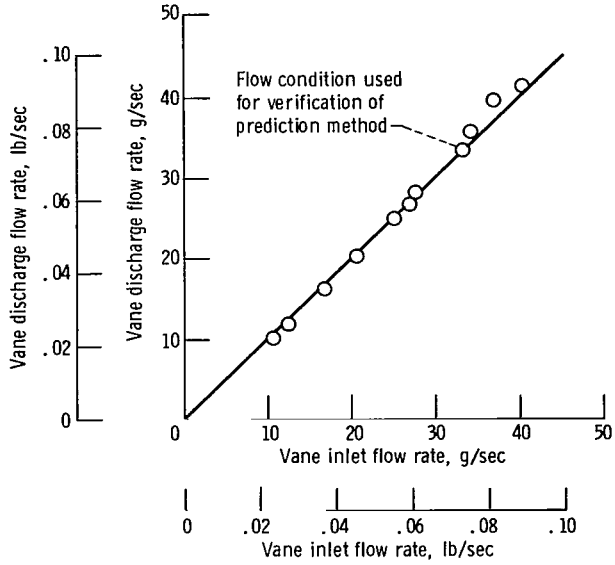

Figure 6. - Comparison of vane inlet and outlet discharge airflow rates.

total vane discharge flow rates were obtained by adding the measured airflows from the probe measurements for each passage and then summing the flow rates for all the passages. Excellent agreement was obtained, as figure 6 illustrates. The maximum discrepancy between inlet and discharge flow rates was 6.5 percent and occurred for the second highest vane flow rate. For the flow condition presented for analytical verification of the prediction method, the agreement between total inlet and discharge flows was within 1 percent.

Orifice Airflow

Discharge coefficients. - Presented in figure 7 are orifice discharge coefficients obtained from experimental data in reference 3 for thick-plate, circular orifices with flow approaching through a perpendicular circular duct. Although this model did not entirely simulate the flow conditions for the orifices in this vane, the low approach Mach numbers made it reasonable to use for the prediction method. For the range of orifice length to diameter ratio (1.6 to 5.6), the orifice discharge coefficients had an essentially constant value of 0.85 for all the passage orifices based on the experimental data shown in figure 7 of reference 3. A discharge coefficient of 0.85 appears generally reasonable and consistent with the experimentally determined curves, which are also shown in figure 7 as a function of orifice Reynolds number for each passage. The exceptions are passages H and I, where the curves are known to be in error because

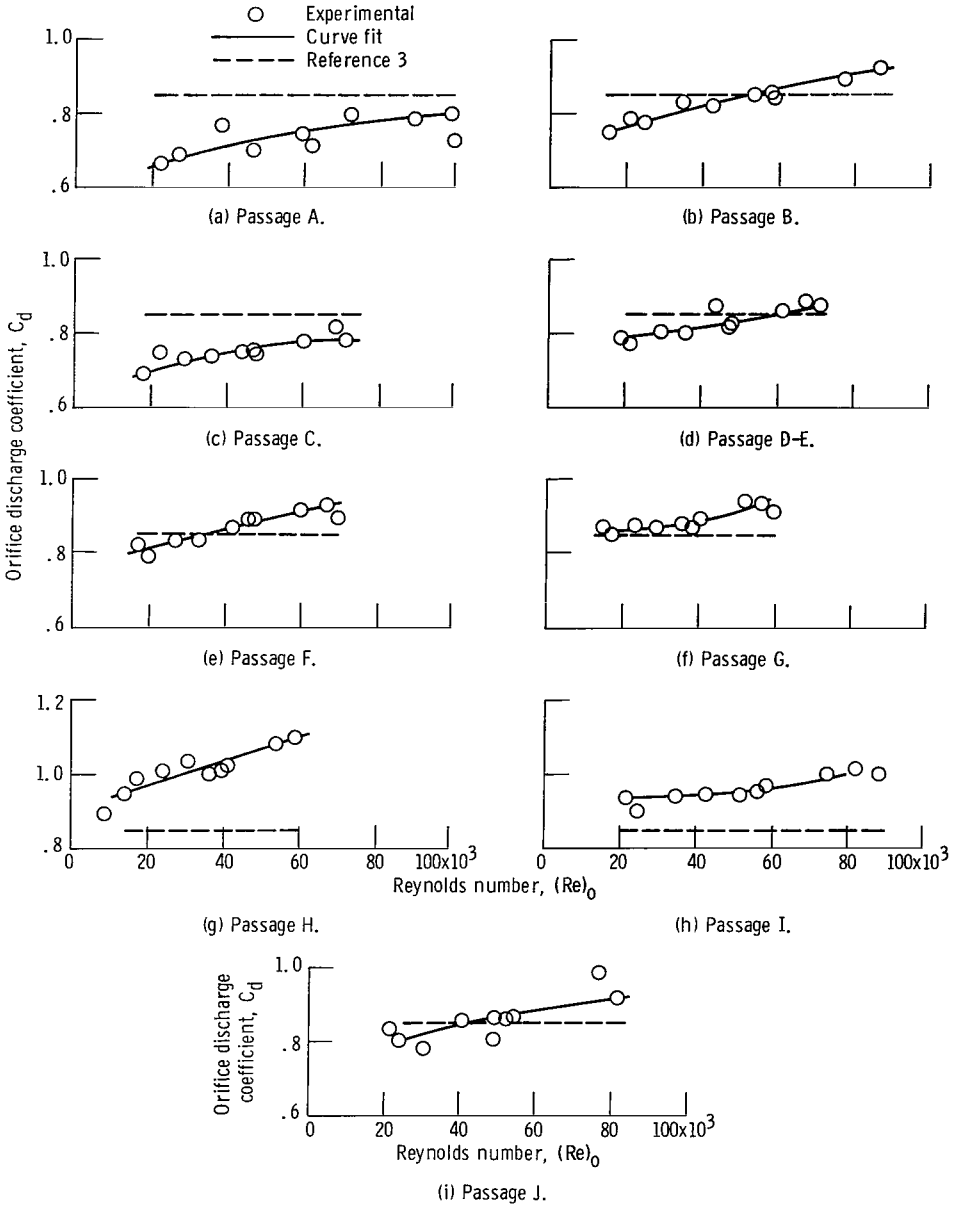

Figure 7. - Orifice discharge coefficients as function of Reynolds number.

they exceed unity. The anomalous discharge coefficient results for these passages are undoubtedly due to the baffle plate not protecting these orifices from the dynamic head of the cooling air entering the plenum from the inlet tube.

Comparison of experimental and predicted orifice flow rates and pressures. - Experimental data and predicted orifice flow rates are summarized in table II. Comparisons are made on the basis of the percent discrepancy between the experimental and predicted results. The largest discrepancies occurred at orifice H (11.5 percent) and

TABLE II. - EXPERIMENTAL AND PREDICTED RESULTS FOR TRANSPIRATION-COOLED VANE WITH TOTAL INLET FLOW RATE OF 32.2 g/sec (0.0731 lb/sec)

Cooling passage	Orifice flow rate					Orifice exit static pressure				
	Experimental		Predicted		Discrepancy, percent	Experimental		Predicted		Discrepancy, percent
	g/sec	lb/sec	g/sec	lb/sec		N/cm^2	psia	N/cm^2	psia	
A	6.53	0.0144	6.94	0.0153	+6.3	18.64	27.04	18.69	27.11	+0.3
B	3.31	.0073	3.18	.0070	-4.1	15.73	22.81	15.99	23.19	+1.7
C	2.31	.0051	2.50	.0055	+7.8	13.52	19.61	14.32	20.77	+5.9
D-E	6.80	.0150	6.80	.0150	0	12.66	18.36	12.83	18.61	+1.4
F	3.81	.0084	3.95	.0087	+3.6	15.76	22.86	12.22	17.73	-22.4
G	2.36	.0052	2.31	.0051	-1.9	14.49	21.01	11.84	17.17	-30.2
H	2.77	.0061	2.45	.0054	-11.5	16.21	23.51	13.84	20.07	-14.6
I	2.72	.0060	2.40	.0053	-11.7	14.78	21.43	13.82	20.04	-6.9
J	2.54	.0056	2.40	.0053	-5.4	13.62	19.76	13.82	20.04	+1.4
Total	33.16	0.0731	32.93	0.0726	-0.7					

orifice I (11.7 percent), where the largest discrepancies also occurred between the measured discharge coefficients and the value of 0.85 which was used. Agreement between predicted and measured flows for the other orifices was within 8 percent. Agreement between the total measured vane inlet flow rate and the total of the predicted orifice flow rates shown in table II was very close; the discrepancy between measured and predicted values was only 0.7 percent.

A comparison is also made in table II of experimental and predicted static pressures at the orifice exit. Agreement between experimental and calculated results is generally good; most of the predicted exit pressures agreed within 7 percent. However, the maximum discrepancy, which occurred at passage G, was about 30 percent. Despite the magnitude of this error in pressure prediction, it is noteworthy that the flow rate in orifice G agreed within 2 percent of the measured flow rate. If, instead of using the data of reference 3, the orifice discharge coefficients had been determined from the curve fits of figure 7, the agreement between predicted and measured results would have been within 6 percent for the flow rates and within 10 percent for the static pressures for all the passage inlets. These comparisons demonstrate that the passage inlet flow rates and pressure can be predicted with generally good accuracy.

Comparison of experimental and predicted passage flow distributions. - Curves of the predicted airflow distribution in each passage are compared with experimental data in figure 8. The measured and calculated flow distributions are in substantial agreement even for passages G, H, and I which previously had the largest discrepancies between predicted and measured passage inlet flows and pressures. Both the predicted

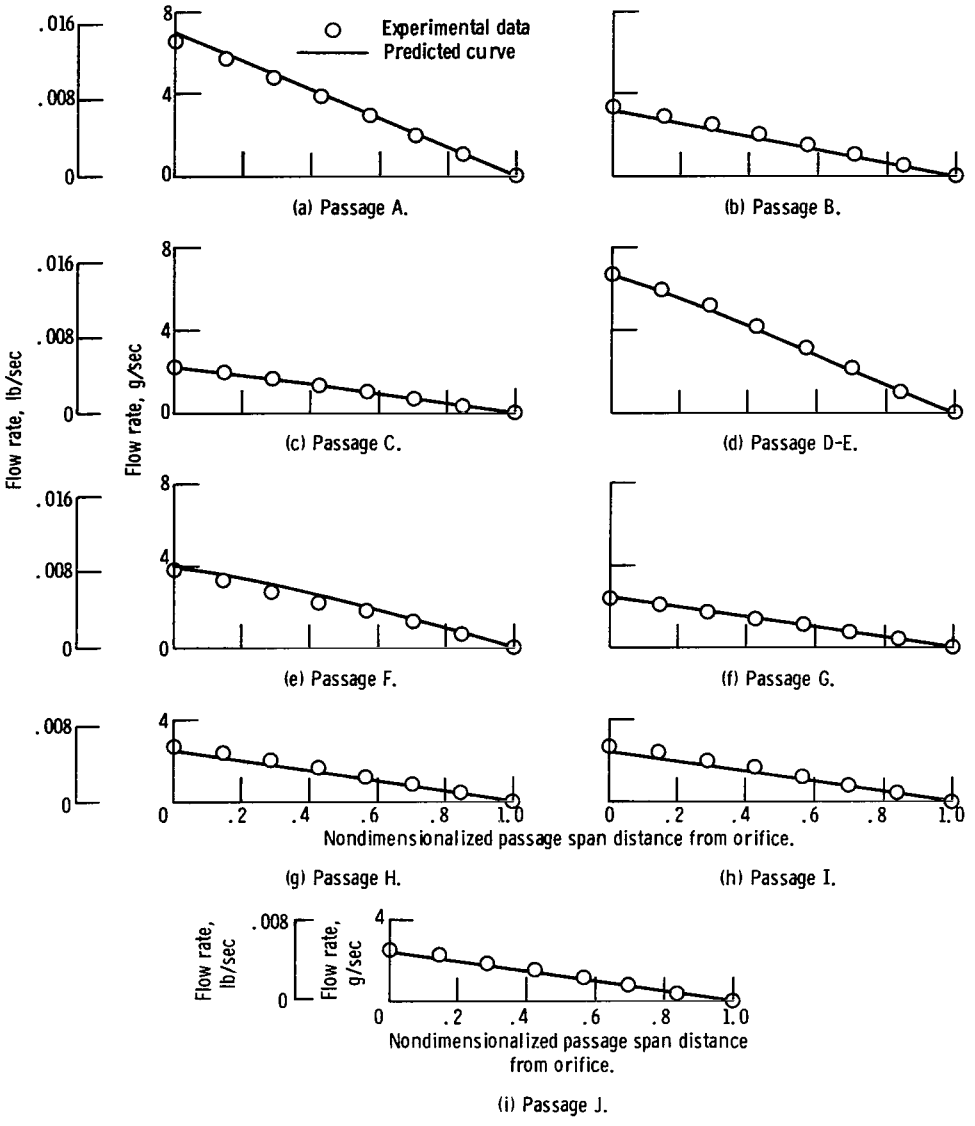

Figure 8. - Airflow distribution in vane coolant passages for inlet flow condition of 33.2 g/sec (0.0731 lb/sec).

and experimental results show that the flow distributions varied almost linearly from the orifice flow rate at station 2 to zero flow at station 4 as a result of the fairly uniform blowing distribution along each passage.

Comparison of experimental and predicted passage pressures. - In figure 9 the measured static pressures at the hub, midspan, and tip of each passage are compared with the calculated static pressure distributions. The solid lines in figure 9 represent the region A of the passage (the static pressure recovery region downstream of the orifice to the point of reattachment). The assumption of a linear static pressure recovery profile resulted in generally good agreement between the calculated curves and

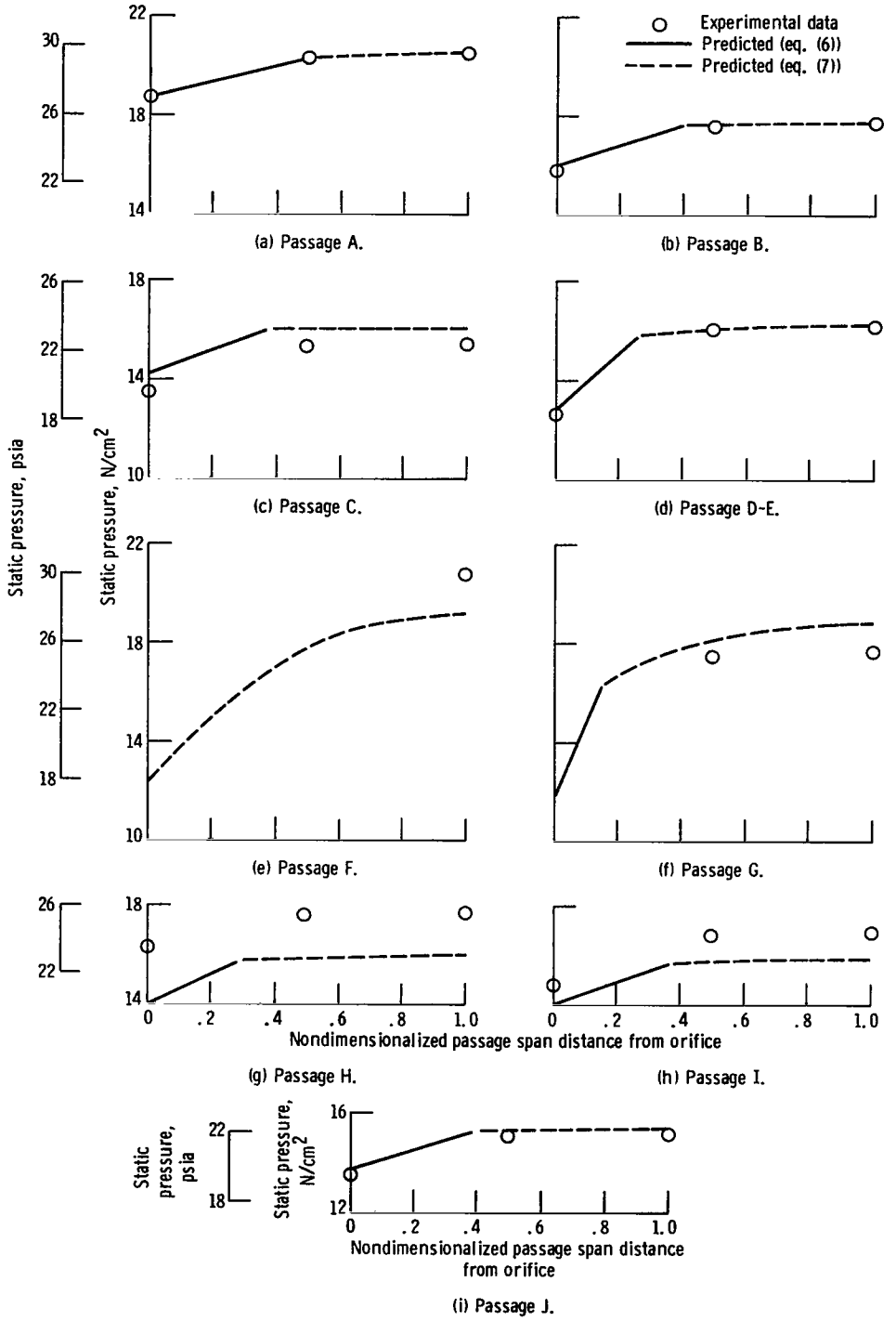

Figure 9. - Static pressure distribution in vane coolant passages for inlet flow condition of 33.2 g/sec (0.0731 lb/sec).

the experimental data for most of the passages.

The calculated pressure distribution in the fully recovered region of the passage (region B) was obtained from equation (7) and is represented by dashed lines in figure 9. In this region, the predicted static pressure increases were less than 0.7 N/cm^2 (1 psi) for the larger passages A, B, C, D-E, H, I, and J. Much higher static pressure changes were predicted for passages F and G because of the higher flow rates per unit area in these small passages.

The midspan static pressure tap in passage F gave faulty readings, and only the tip and hub pressures are plotted in figure 9(f). As mentioned previously, the orifice and passage areas of passage F were equal and, as a result, there was no region A of flow reattachment; therefore, the entire passage was treated as fully developed flow.

The inability to predict the correct shape or level of the pressure profiles in passages F and G is probably caused by deviations between as-fabricated and design passage dimensions. The most sensitive passage dimension is the discharge flow width of the porous side. Calculations have shown that a 10 percent error in the flow width of passage G would be equivalent to a 35 percent error in passage area.

The discrepancies between calculated pressures and experimental data for passages H and I are due to the differences between the discharge coefficients determined from reference 3 and the experimentally obtained curve fits for orifices H and I shown in figure 7. As discussed previously, these orifices showed fictitiously high orifice discharge coefficients because a small error in positioning the inlet baffle plate permitted direct impingement of the cooling air on these orifices.

At the conclusion of the experimental program, the vane was cut at the hub, midspan, and tip sections; and photographic enlargements (10 times size) were made of these sections. Measurements taken from these enlargements generally agreed within 8 percent with the passage dimensions given in table I. The largest discrepancy between the measured dimensions and those used in the calculations occurred at passage F, largely because the area of this passage was found to taper from tip to hub by a factor of 2. However, many of the other measurements were considered to be of doubtful value since the grinding of the airfoil caused some breakage of welds and partial distortion or separation of the porous skin from the strut.

A possibility existed that some of the discrepancies between measured and predicted pressures in figure 9 could be caused by local variations in the flow characteristics of the porous shell. This was ruled out, however, by calculations which showed no significant differences in predicted flows and pressures when the local α and β values, as determined from vane flow tests, were used instead of the nominal values obtained from the equations of reference 6.

When this vane was designed (ref. 7), an assumption was made that the passages behave as plenums with no change in static pressure in the spanwise direction. That

this is not the case is obvious from the prediction analysis and experimental data presented in this report. A design that neglects this static pressure rise in the strut passages will not predict the correct blowing distribution. In fact, neglecting the low-pressure region just downstream from the orifice may result in a design which does not provide adequate transpiration cooling in this region or may result in ingestion of the hot gas stream during engine operation.

Porous Shell Discharge Airflow

The measured and predicted airflows discharging from each coolant passage through the vane porous shell are presented in figure 10 in bar chart form for each of the seven span increments over which discharge flow measurements were made. There was a general trend for the discharge flow rates to increase with span distance. This trend resulted from the increase in static pressure from the tip to hub of the passage and was most marked for those passages which showed the sharpest rises in pressure, such as D-E (fig. 9(d)) and F (fig. 9(e)).

Comparison of the measured and predicted local discharge flow rates shown in figure 10 indicate reasonably good agreement. The largest discrepancy between experiment and prediction was about 30 percent and occurred locally in passage F. In this case, the experimental discharge flow rates were questionable because of fabrication errors which resulted in a tapered passage area and therefore an unknown porous wall flow width. Other passages which show noticeable disagreement in figure 10 are C, H, and I; it is noteworthy that these were the very passages which also showed poor agreement in figure 7. The correlation between experimental and calculated local discharge flow rates is good, as shown in figure 10, considering the small flow rates involved and the possible experimental errors, which include inaccuracies in flow and pressure measurements, incorrect passage and orifice geometries, and misplacement of the vane inlet baffle plate.

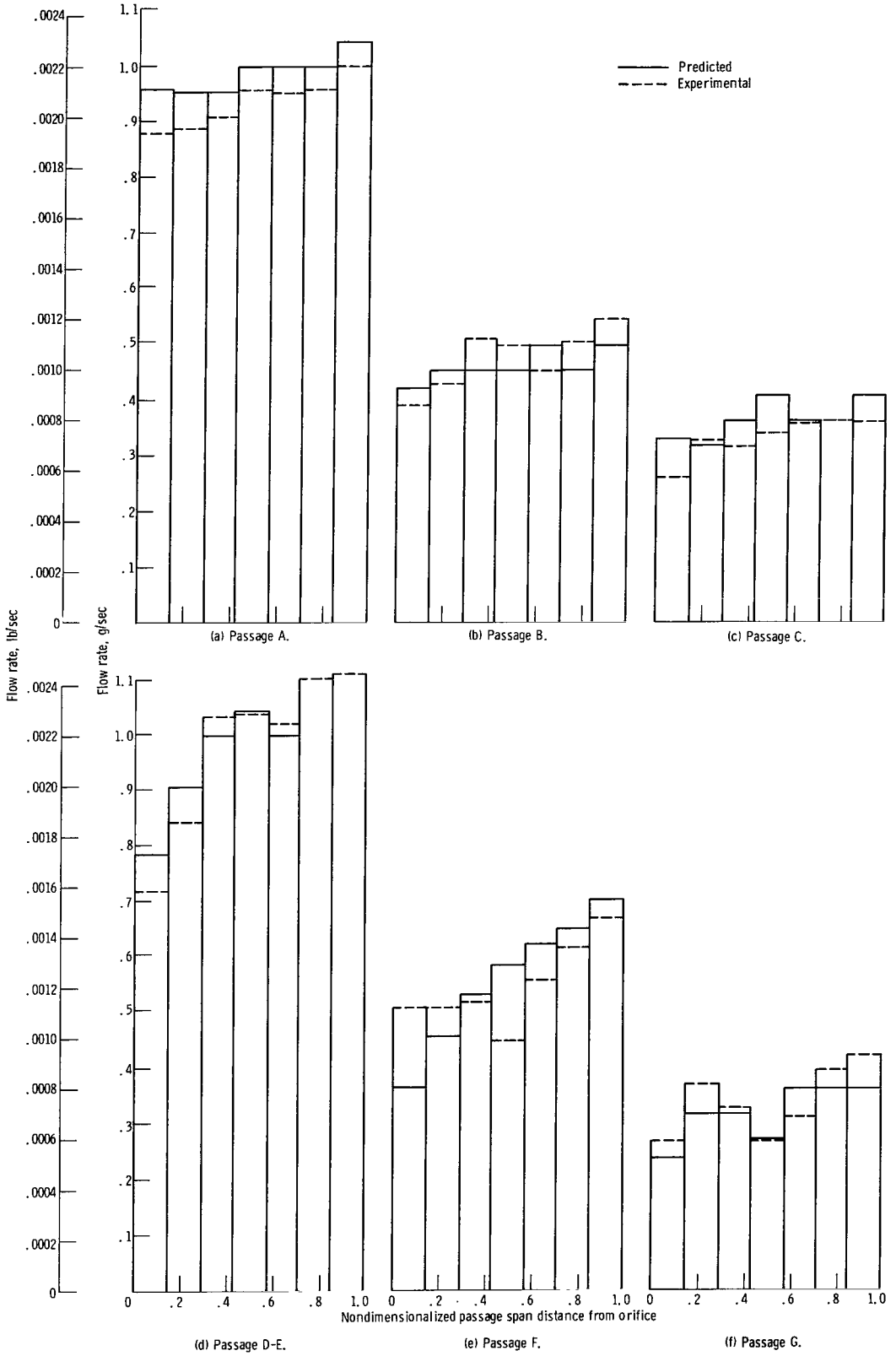

Figure 10. - Comparison of predicted and experimental discharge flow rates through porous shell of vane.

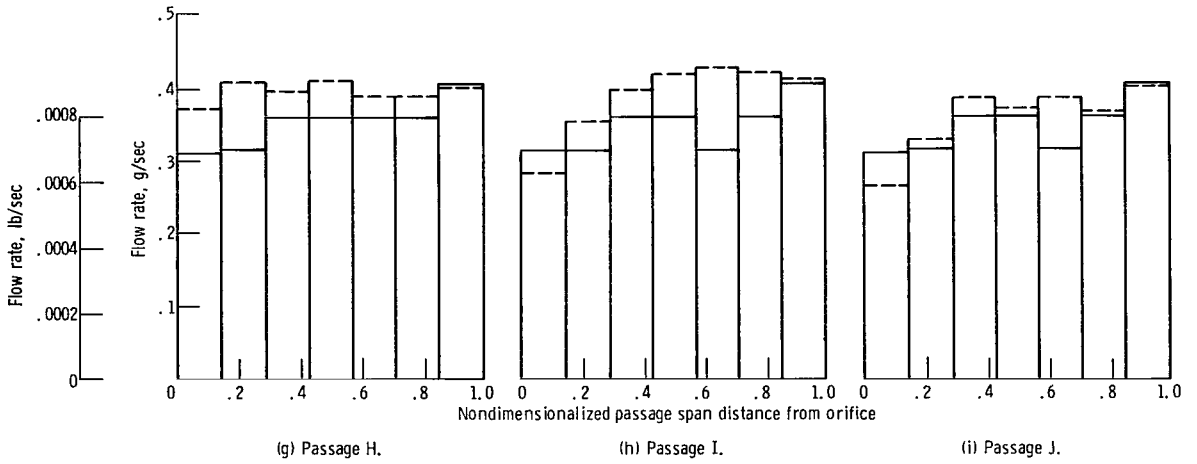

(g) Passage H. (h) Passage I. (i) Passage J.

Figure 10. - Concluded.

SUMMARY OF RESULTS

The results of this investigation can be summarized as follows:

1. Total airflow into the vane was predicted within 1 percent and flow distribution into the various coolant passages was predicted within 12 percent by using a one-dimensional compressible flow analysis.

2. Flow rate and static pressure distributions within the coolant passages and discharge flows through the porous shell were successfully predicted. The largest discrepancies between predicted and experimental results generally occurred for passages where errors in vane fabrication were known to be involved.

3. Orifice discharge coefficients obtained from empirical results presented by Rohde, Richards, and Metger showed generally good agreement with discharge coefficients obtained from vane flow tests. Two passages directly beneath the inlet tube resulted in discharge coefficients that were too high; this was caused by the dynamic head of the inlet flow. The accuracy of the flow and pressure predictions could be appreciably improved by using the orifice discharge coefficients determined from vane tests.

4. Nominal porous material flow characteristics obtained from empirical equations presented by Kaufman and Richards proved suitable for flow and pressure predictions.

Lewis Research Center,
National Aeronautics and Space Administration,
Cleveland, Ohio, May 23, 1972,
764-74.

REFERENCES

1. Calvert, Howard F.; Cochran, Reeves P.; Dengler, Robert P.; Hickel, Robert O.; and Norris, James W.: Turbine Cooling Research Facility. NASA TM X-1927, 1970.

2. Clark, John S.; Richards, Hadley T.; Poferl, David J.; and Livingood, John N. B.: Coolant Pressure and Flow Distribution Through an Air-Cooled Vane for a High-Temperature Gas Turbine. NASA TM X-2028, 1970.

3. Rohde, John E.; Richards, Hadley T.; and Metger, George W.: Discharge Coefficients for Thick Plate Orifices with Approach Flow Perpendicular and Inclined to the Orifice Axis. NASA TN D-5467, 1969.

4. Benedict, R. P.; Carlucci, N. A.; and Swetz, S. D.: Flow Losses in Abrupt Enlargements and Contractions. J. Eng. Power, vol. 88, no. 1, Jan. 1966, pp. 73-81.

5. Green, L., Jr.; and Duwez, P.: Fluid Flow Through Porous Metals. J. Appl. Mech., vol. 18, no. 1, Mar. 1951, pp. 39-45.

6. Kaufman, Albert; and Richards, Hadley T.: Investigation of Flow Characteristics of Some Wire-Form and Laminate-Form Porous Materials. NASA TM X-2111, 1970.

7. Nealy, D. A.; and Anderson, R. D.: Design of a Strut Supported Turbine Vane With a Wire-Form Porous Shell. Rep. CDR-5923, General Motors Corp. (NASA CR-72508), July 15, 1968.

8. Turner, A. B.: Heat Transfer Characteristics of Transpiration Cooled Gas Turbine Blades. Ph.D. Thesis, University of Sussex, June 1968.

NASA-Langley, 1972 —— 2 E-6800

"The aeronautical and space activities of the United States shall be conducted so as to contribute . . . to the expansion of human knowledge of phenomena in the atmosphere and space. The Administration shall provide for the widest practicable and appropriate dissemination of information concerning its activities and the results thereof."

—NATIONAL AERONAUTICS AND SPACE ACT OF 1958

NASA SCIENTIFIC AND TECHNICAL PUBLICATIONS

TECHNICAL REPORTS: Scientific and technical information considered important, complete, and a lasting contribution to existing knowledge.

TECHNICAL NOTES: Information less broad in scope but nevertheless of importance as a contribution to existing knowledge.

TECHNICAL MEMORANDUMS: Information receiving limited distribution because of preliminary data, security classification, or other reasons.

CONTRACTOR REPORTS: Scientific and technical information generated under a NASA contract or grant and considered an important contribution to existing knowledge.

TECHNICAL TRANSLATIONS: Information published in a foreign language considered to merit NASA distribution in English.

SPECIAL PUBLICATIONS: Information derived from or of value to NASA activities. Publications include conference proceedings, monographs, data compilations, handbooks, sourcebooks, and special bibliographies.

TECHNOLOGY UTILIZATION PUBLICATIONS: Information on technology used by NASA that may be of particular interest in commercial and other non-aerospace applications. Publications include Tech Briefs, Technology Utilization Reports and Technology Surveys.

Details on the availability of these publications may be obtained from:

SCIENTIFIC AND TECHNICAL INFORMATION OFFICE

NATIONAL AERONAUTICS AND SPACE ADMINISTRATION

Washington, D.C. 20546